Discrete modeling of strain accumulation in granular soils under low amplitude cyclic loading

Ngoc-Son Nguyen*, Stijn François, Geert Degrande

KU Leuven, Department of Civil Engineering, Kasteelpark Arenberg 40, B-3001 Leuven, Belgium

Abstract

An advanced understanding of the strain accumulation phenomenon in granular soils subjected to low amplitude cyclic loading with relatively high frequency is needed to enhance the ability to predict the settlement of granular soils induced by vibrations. In the current study, the discrete element method is used to study this phenomenon. A loose and a medium dense sample composed of a relatively large number of spheres are considered. A series of stress controlled cyclic triaxial tests with different excitation amplitudes and frequencies is performed on these samples at different static stress states. The response of these samples at the macroscopic and microscopic scales is analyzed. The sample density, the cyclic stress amplitude and the static stress state importantly affect strain accumulation. However, the cyclic excitation frequency has a small effect on strain accumulation. At the microscopic scale, frictional sliding occurring at a few contacts continuously dissipates energy and the fraction of these contacts varies periodically during cyclic loading. The coordination number of these samples increases slightly as strain accumulates. However, the anisotropy remains almost constant during low amplitude cyclic excitation. A qualitatively good agreement between numerical and experimental results is found.

Keywords: Granular soils, cyclic loading, low amplitude, high frequency, strain accumulation, discrete element method

1. Introduction

Granular soils under the foundation of buildings are subjected to vibrations arising from several sources such as road and railway traffic, construction activities and reciprocating machines. Vibrations cause the stress state in these media to vary cyclically with low amplitude compared to the static stress state. The excitation frequency can be typically up to 20 Hz for road traffic induced vibrations [1] and 150 Hz for railway traffic induced vibrations [2]. Due to hysteresis, each loading cycle results in a small residual deformation. This deformation accumulates with increasing number of cycles and may become significant after a large number of cycles, causing differential settlement of soils under foundations and hence damage to buildings. Several phenomenological models have been proposed to predict the differential settlement of granular media subjected to low amplitude cyclic loading [3–6], which are based on a large number of laboratory experiments. These models present significant drawbacks as some of their parameters do not have a clear physical meaning and are difficult to identify. Consequently, there is still an increasing need to advance the understanding of strain accumulation in granular materials under low amplitude cyclic loading and the ability to predict this phenomenon.

Many laboratory experiments have been conducted to study strain accumulation in granular media under cyclic loading. Wichtmann et al. [7, 8] performed a complete experimental study of strain accumulation in

*Corresponding author

Email addresses: ngocson.nguyen@bwk.kuleuven.be (Ngoc-Son Nguyen), stijn.francois@bwk.kuleuven.be (Stijn François), geert.degrande@bwk.kuleuven.be (Geert Degrande)

Postprint submitted to Computers and Geotechnics
Published version:
N. Nguyen, S. François, and G. Degrande. Discrete modeling of strain accumulation in granular soils under low amplitude cyclic loading. *Computers and Geotechnics*, 62:232–243, 2014. http://dx.doi.org/10.1016/j.compgeo.2014.07.015

sand samples: low amplitude cyclic triaxial tests with a large number of cycles (up to 10^5) were conducted at low frequencies varying from 0.05 Hz to 2 Hz. It was shown that strain accumulation in sand samples depends on several factors such as the sample density, the cyclic stress amplitude, the cyclic frequency, the average stress, the loading history and the grain size distribution. Cyclic triaxial tests on sand samples at higher frequencies were performed by Karg [6] and Rascol [9]. Karg has found that strain accumulation is not influenced by loading frequencies ranging from 2 to 10 Hz. His study turned out, however, that the performance of cyclic tests is significantly reduced at frequencies above 2 Hz as the pneumatic loading system could not follow exactly the sinusoidal loading curve. Suiker [10] and Indraratna et al. [11] studied strain accumulation in ballast samples through high amplitude cyclic triaxial tests at frequencies up to 40 Hz. These studies showed that strain accumulation in ballast samples is not influenced by cyclic frequencies under 5 Hz [10], but it is importantly influenced by frequencies ranging from 10 to 40 Hz [11].

The discrete element method (DEM) pioneered by Cundall and Strack [12] can complement laboratory experiments. O'Sullivan [13] gives a full description of this method. The DEM is able to simulate complex loading tests which are difficult to conduct experimentally and enables access to information at the particle level so the local behavior at the particle scale can be investigated. This method has been widely used to simulate monotonic and cyclic loading tests. Most of cyclic loading tests were performed with high amplitude. Alonso-Marroquín et al. [14, 15] simulated cyclic tests with large amplitude on assemblies of polygons to study the ratcheting phenomenon in granular media. A few simulations of low amplitude cyclic tests are found. Recently, Hu et al. [16, 17] have reported numerical simulations of low amplitude cyclic biaxial tests at constant mean stress on 2D loose granular samples composed of a relatively small number (896) of disks. They focused on the evolution of the internal structure of 2D granular media during low amplitude cyclic loading at low frequencies (< 1 Hz). The effect of the average stress state and cyclic stress amplitude on the accumulation of the axial strain was also analyzed. It was not shown, however, how these factors influence the accumulation of the volumetric and deviatoric strains and the direction of strain accumulation.

The present paper presents a study of strain accumulation in 3D granular samples under the action of traffic induced vibrations by simulating low amplitude cyclic triaxial tests at relatively high frequency. While it is difficult to conduct low amplitude cyclic tests at high frequency in the laboratory, the DEM is an alternative option to simulate this kind of cyclic tests. Moreover, this method allows an investigation of the microscopic behavior of granular samples during cyclic excitation. The first purpose of the current study is to analyze the influence of different factors such as the sample density, the amplitude and the frequency of the cyclic excitation and the static stress state on strain accumulation in granular soils. For this purpose, the DEM has a great advantage compared to laboratory experiments since different loadings can be applied on the same sample. The second purpose is to investigate the energetic behavior and the evolution of the internal structure of granular materials during low amplitude cyclic loading. The main novelty of the current study compared to the study of Hu et al. [16, 17] resides in the high frequency of cyclic loading and the more detailed analysis of strain accumulation. In addition, 3D samples considered in the current study reproduce better the packing density and the deformation of real granular materials and allow a confrontation between numerical results and experimental data reported in [7, 8].

This paper is organized as follows. Section 2 presents two numerical samples considered in the current study. The behavior of these samples during triaxial compression tests is briefly discussed in section 3. Strain accumulation in these samples during low amplitude cyclic triaxial tests and the influence of different parameters on this phenomenon are analyzed in section 4.

2. Numerical samples

The software PFC3D [18] is used to simulate low amplitude cyclic triaxial tests on 3D granular samples. To simulate a large number of loading cycles within a reasonable computation time, spherical non-crushable particles, a linear contact model and a rigid wall boundary are adopted in the current study. Two samples A and B with different densities are created, each of which is composed of 10342 spheres with mass density $\rho = 2650$ kg/m^3. The particle size for both samples is uniformly distributed from $d_{\min} = 4$ mm to $d_{\max} = 8$ mm. This particle size is larger than that of actual sand samples whose maximum grain diameter is about

2 mm. In the DEM, the time step is proportional to the square root of the particle mass. As a result, a very small time step (typically of the order 10^{-7} s) is required to simulate samples with particle size smaller than 2 mm; therefore, computation time is very long. Samples A and B correspond actually to fine gravels. They are used to keep computation time reasonable.

The parameters of the linear contact model are the normal and tangential stiffnesses $k_{\mathrm{n}} = k_{\mathrm{s}} = 5 \times 10^6$ N/m and the friction coefficient $\mu = 0.6$. No viscous damping is added at the contact points; therefore, only friction dissipates energy in the samples. To justify the quasi-rigidity assumption for particles, the ratio $k_n/(\sigma_o d)$ with σ_o the confinement stress and d the mean particle diameter must be sufficiently high. In the current study $\sigma_o \leq 100$ kPa hence $k_n/(\sigma_o d) > 8 \times 10^3$ which is acceptable. The resulting time step is of the order 10^{-6} s.

The particles of each sample are randomly generated in a parallelepiped composed of 6 rigid walls. The samples are then isotropically compacted until reaching a given target stress state. To obtain different densities, the friction coefficient μ for samples A and B is set to 0.6 and 0.3 during the compaction phase, respectively. When about 90% of the target stress state is reached, μ is reset to its original value. Figure 1 shows sample A after compaction with height $H = 17.0$ cm and width $L = 11.4$ cm.

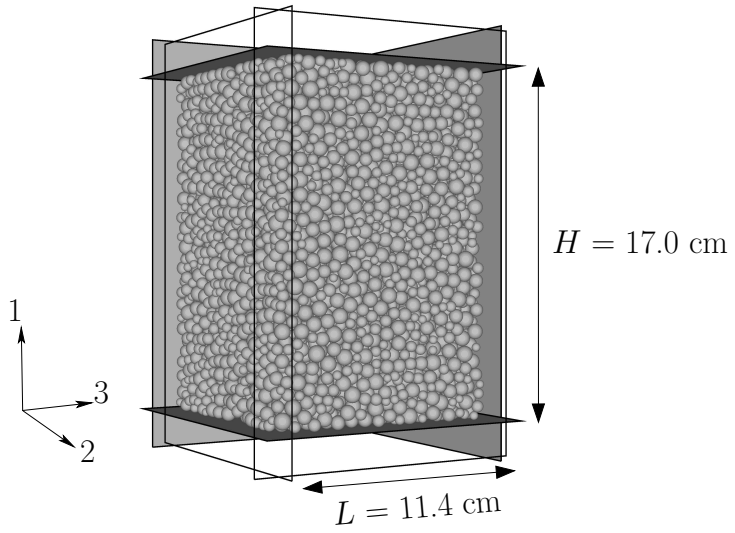

Figure 1: Configuration of sample A contained by a parallelepiped box composed of 6 rigid walls.

Particle breakage might occur in granular materials during cyclic loading, particularly at high amplitude and high hydrostatic stress [11, 19]. It can be expected that only a small number of particles would be crushed during low amplitude cyclic loading at low hydrostatic stress. As indicated in [10], particle breakage is indeed small in ballast samples subjected to high amplitude cyclic loading tests at a hydrostatic stress $p < 193$ kPa. Donohue et al. [19] observed that the amount of particle breakage in carbonate sand, which is quite fragile, is small during cyclic loading tests at a hydrostatic stress $p = 100$ kPa. Consequently, it is relevant to neglect particle breakage in the current study.

The rigid wall boundary is used in the current study as it is easily implemented and a small computational effort is needed. However, this rigid boundary inhibits the natural development of shear bands that are clearly observed during physical triaxial compression tests. To enable shear bands to develop, a stress controlled membrane has been introduced in [20, 21], which simulates the flexible latex membrane used in physical tests. However, the implementation of this membrane boundary is quite complex, in particular for 3D materials, and a significant computational effort is needed to update it during simulation. The stress controlled membrane has been used by Hu et al. [17] to simulate low amplitude biaxial cyclic tests on 2D materials. When the membrane boundary is used, only the post-peak response (after the failure) of granular

samples during a triaxial compression differs notably from that obtained with the rigid wall boundary [21]. As a result, it can be expected that, for low amplitude cyclic tests, the rigid wall boundary and the membrane boundary give close results as cyclic excitations are applied before the failure limit.

Characteristics of samples A and B

The stress tensor $\boldsymbol{\sigma}$ and strain tensor $\boldsymbol{\varepsilon}$ of each sample are defined from the contact forces applied by the walls on the sample and the displacement of the walls [13]. The sign convention used in this paper is that tensile stresses and strains are positive. For triaxial loading, the mean stress p and the deviatoric stress q are defined as $p = (\sigma_{11} + 2\sigma_{33})/3$ and $q =\mid \sigma_{11} - \sigma_{33} \mid$. The volumetric strain ε_{v} and the deviatoric strain ε_{d} are defined as $\varepsilon_{\mathrm{v}} = \varepsilon_{11} + 2\varepsilon_{33}$ and $\varepsilon_{\mathrm{d}} = 2 \mid \varepsilon_{11} - \varepsilon_{33} \mid /3$.

The coordination number $\overline{N}$ and the fabric tensor $\boldsymbol{H}$ are used to describe the internal structure of each sample. The coordination number $\overline{N}$ is the average number of contacts per particle

$$\overline{N} = 2\frac{N_{\mathrm{c}}}{N_{\mathrm{p}}}, \tag{1}$$

with N_{c} the number of contacts and N_{p} the number of particles. Kuhn [22] introduced the effective coordination number $\overline{N}_{\mathrm{eff}}$ by removing all the floating particles (particles that have no more than 3 contacts with their neighbors) from the sample when calculating the coordination number $\overline{N}$. The fabric tensor is defined as:

$$H_{ij} = \frac{1}{N_{\mathrm{c}}} \sum_{k=1}^{N_{\mathrm{c}}} n_i^k n_j^k, \tag{2}$$

where n_i^k is the i-th component of the unitary normal vector at contact k [23]. For triaxial loading, H_{11}, H_{22} and H_{33} are the three principal values and $H_{22} \approx H_{33}$. In this case, the anisotropy of a sample can be measured by $H_{\mathrm{d}} = H_{11} - H_{33}$.

Sample	n	$\overline{N}$	$\overline{N}_{\mathrm{eff}}$	H_{d}
A	0.427	3.20	4.36	0.01
B	0.409	3.60	4.60	0.01

Table 1: Porosity n, coordination number $\overline{N}$, effective coordination number $\overline{N}_{\mathrm{eff}}$ and anisotropy measure H_{d} of samples A and B at a confinement stress $\sigma_o = 50$ kPa.

Table 1 presents some characteristics of samples A and B at the end of the compaction phase for an isotropic stress state $\sigma_{11} = \sigma_{22} = \sigma_{33} = \sigma_o = 50$ kPa. Sample B is denser than sample A. Moreover, for each sample the effective coordination number $\overline{N}_{\mathrm{eff}}$ is significantly higher than $\overline{N}$. Both samples are approximately isotropic. The following sections show that the difference in density of these samples leads to a marked difference in their behavior during triaxial compression tests and cyclic triaxial tests.

3. Triaxial compression tests

Quasi-static triaxial compression tests are performed on samples A and B by approaching slowly the top and bottom walls and keeping the lateral stresses σ_{22} and σ_{33} equal to the confinement stress σ_o using a servo-control procedure. Figure 2 shows the stress ratio $\eta = q/ \mid p \mid$ and the volumetric strain ε_{v} versus the axial strain ε_{11} for two tests performed on samples A and B at $\sigma_{\mathrm{o}} = 50$ kPa. Data obtained from the numerical simulation are relatively noisy, particularly for the computed stress. Therefore, the Savitzky-Golay filtering method is used to smooth the data. The figure shows that sample A presents the behavior of a loose granular sample, while sample B presents the behavior of a medium dense one. These samples first contract and then dilate. The state at which this transition occurs is called the characteristic state (phase transformation state). For sample A the characteristic state occurs at large deformation ($\varepsilon_{11} \approx$ -0.074),

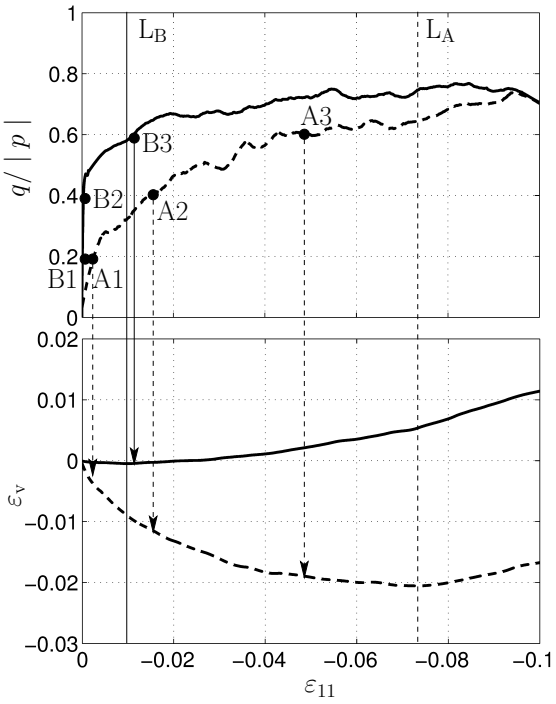

Figure 2: Stress ratio $\eta = q/\mid p \mid$ and volumetric strain ε_{v} versus axial strain ε_{11} for two triaxial compression tests applied on samples A (dashed line) and B (solid line) at a confinement stress $\sigma_{\mathrm{o}} = 50$ kPa.

while for sample B this state occurs at small deformation ($\varepsilon_{11} \approx$ -0.009). Lines $\mathrm{L_A}$ and $\mathrm{L_B}$ drawn in figure 2 depict the characteristic state for samples A and B, respectively. The stress ratio η at the characteristic state is higher for sample A (0.67) than for sample B (0.59). This result is in good agreement with the findings in [24].

Points A1, A2 and A3 drawn on the curve for sample A and points B1, B2 and B3 drawn on the curve for sample B represent the stress states at which low amplitude cyclic excitations are applied (these loadings are presented in section 4). The arrows indicate the volumetric behavior of each sample at the corresponding stress states. At each point, the volumetric behavior of the corresponding sample is quantified by the dilatancy rate $\dot{\varepsilon}_{\mathrm{v}}/\dot{\varepsilon}_{\mathrm{d}}$ which is negative if the sample is contracting. Table 2 shows the stress ratio η and the dilatancy rate $\dot{\varepsilon}_{\mathrm{v}}/\dot{\varepsilon}_{\mathrm{d}}$ at these points. Sample A tends to contract less from point A1 to point A3; the same tendency is observed for sample B from point B1 to point B3. In particular, at point B3, sample B slightly dilates. It is shown in the next section that samples A and B behave differently during the cyclic excitations applied at these points.

4. Low amplitude cyclic triaxial tests

The cyclic triaxial tests presented in this paper are performed in a stress controlled manner. The axial stress σ_{11} is cycled between the lower and upper values $\overline{\sigma}_{11} \pm \sigma_{11}^{\mathrm{cyc}}$ where $\overline{\sigma}_{11}$ is the average or static axial stress and $\sigma_{11}^{\mathrm{cyc}}$ is the cyclic axial stress amplitude. The lateral stresses σ_{22} and σ_{33} are kept equal to the confinement stress σ_{o}. The phase in which the stress state is brought to the average stress state ($\sigma_{11} = \overline{\sigma}_{11}$ and $\sigma_{22} = \sigma_{33} = \sigma_{\mathrm{o}}$) is called the consolidation phase. In the current study, a sample is consolidated by performing a triaxial compression test. Once the target average stress state has been reached, the cyclic stress σ_{11} is applied by moving cyclically the top and bottom walls inward and outward until σ_{11} reaches the upper and lower values, respectively. The velocity of these walls is changed smoothly to avoid shocks

Sample	Point	η	$\dot{\varepsilon}_{\rm v}/\dot{\varepsilon}_{\rm d}$
	A1	0.2	-0.7
A	A2	0.4	-0.26
	A3	0.6	-0.16
	B1	0.2	-0.4
B	B2	0.4	-0.06
	B3	0.6	0.01

Table 2: Stress ratio η and dilatancy rate $\dot{\varepsilon}_{\rm v}/\dot{\varepsilon}_{\rm d}$ of samples A and B at points A1, A2, A3, B1, B2 and B3 in figure 2.

to the samples. By doing so, the amplitude $\sigma_{11}^{\rm cyc}$ can be controlled exactly; however, a sinusoidal stress excitation with a given frequency cannot be correctly applied due to the difficulty in choosing the velocity of the top and bottom walls to reach a given value of σ_{11} at a given instant t. This is a significant limitation of using rigid walls without mass to confine granular samples because the force cannot be applied on massless bodies. Indraratna et al. [11] report to have developed a subroutine in the software PFC2D to apply a stress controlled cyclic biaxial test with a given amplitude and frequency but give no implementation detail. In the current study, the frequency f of a cyclic excitation is an average value computed as $f = \mathcal{N}/T_{\rm f}$ with $\mathcal{N}$ the number of cycles and $T_{\rm f}$ the duration of the test. The frequency f is approximately controlled within a given range by trial and error.

A cyclic triaxial test has four parameters: the average stress ratio $\overline{\eta} = \overline{q}/\mid \overline{p} \mid$, the confinement stress $\sigma_{\rm o}$, the cyclic stress amplitude $\sigma_{11}^{\rm cyc}$ and the excitation frequency f. A low amplitude cyclic excitation corresponds to a small value of the ratio $\zeta^{\rm cyc} = \sigma_{11}^{\rm cyc}/\mid \overline{p} \mid$. Table 3 summarizes the parameters of the cyclic triaxial tests performed on samples A and B.

In DEM simulations, the number of particles in a sample should be large enough such that the sample is representative. One way to check the representativity of a sample composed of a given number of particles is to increase the number of particles. The sample is representative if its behavior does not significantly change. To do so, four samples composed of 6000, 8000, 10000 and 12000 spheres with porosities close to 0.416 are created and then subjected to the same cyclic triaxial loading test with $\overline{\eta} = 0.4$, $\sigma_{\rm o} = 50$kPa, $\sigma_{11}^{\rm cyc}$ = 6kPa and $f \approx 67$ Hz. The magnitude $\varepsilon^{\rm acc}$ of the accumulated strain is defined as the Frobenius norm of the accumulated strain tensor $\boldsymbol{\varepsilon}^{\rm acc}$. For cyclic triaxial loading, $\boldsymbol{\varepsilon}^{\rm acc}$ is diagonal; therefore, $\varepsilon^{\rm acc} = \|\boldsymbol{\varepsilon}^{\rm acc}\|_{\rm F} = \sqrt{(\varepsilon_{11}^{\rm acc})^2 + (\varepsilon_{22}^{\rm acc})^2 + (\varepsilon_{33}^{\rm acc})^2}$. Figure 3 shows the accumulated strain $\varepsilon^{\rm acc}$ in these four samples versus the cycle number $\mathcal{N}$. The accumulated strain in the sample of 10000 particles is quite different from that in the samples of 6000 and 8000 particles but close to that in the sample of 12000 particles. This result reveals that, for cyclic triaxial loading test, the samples composed of 10000 particles used in our simulations are representative.

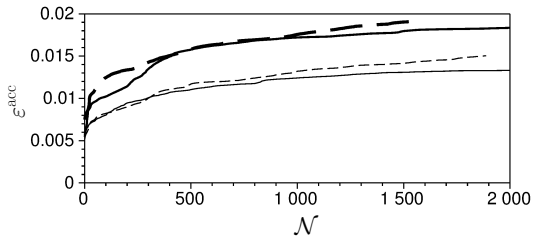

Figure 3: Accumulated strain $\varepsilon^{\rm acc}$ versus the cycle number $\mathcal{N}$ for four samples composed of 6000 (thin solid line), 8000 (thin dashed line), 10000 (bold solid line) and 12000 (bold dashed line) particles.

Sample	Test	$\overline{\eta}$	σ_o (kPa)	σ_{11}^{cyc} (kPa)	f (Hz)
A	A1	0.2	50	6	62
	A2	0.4		3	25
	A3			6	24
	A4				67
	A5				93
	A6			12	30
	A7		100		66
	A8	0.6	50	6	67
B	B1	0.2	50	6	63
	B2	0.4			25
	B3				68
	B4				100
	B5	0.6			66

Table 3: Cyclic triaxial tests performed in the current study.

In the following, test B2 is first presented in subsection 4.1 to demonstrate strain accumulation in sample B. Next, the influence of the sample density, the cyclic stress amplitude σ_{11}^{cyc}, the cyclic excitation frequency f, the average stress ratio $\overline{\eta}$ and the confinement stress σ_o on strain accumulation is analyzed in subsections 4.2 to 4.6.

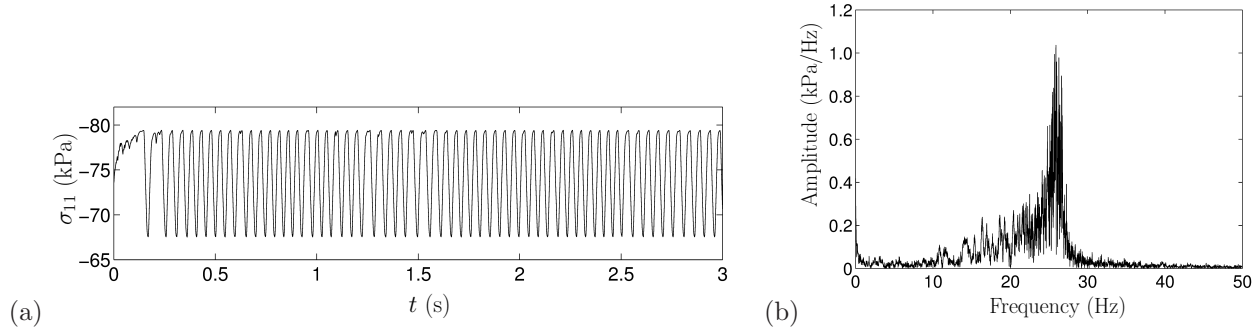

Figure 4: (a) Time history and (b) frequency content of the cyclic axial stress σ_{11} applied in test B2.

4.1. Test B2

Figure 4 shows the time history and frequency content of the cyclic axial stress σ_{11} applied on sample B in test B2. The stress σ_{11} is not perfectly sinusoidal as mentioned previously and its dominant frequency is about 25 Hz.

The stress-strain response of the sample under the applied cyclic excitation is shown in figure 5. For clarity, this plot is split into three subplots with equal intervals of the axial strain ε_{11}. This figure shows clearly that sample B accumulates strain during cyclic excitation even at small amplitude. The first two

cycles involve a large accumulated strain. The strain accumulation slows down as the cyclic loading continues. However, at several moments the strain accumulation suddenly accelerates and then rapidly stabilizes. At these moments, internal instability might occur in the sample, which is most likely due to the collapse of some strong force chains that carry essentially the deviatoric stress in the sample as explained by Hu et al. [17]. Afterwards, a particle rearrangement is triggered to create new strong force chains and the sample recovers its bearing capability. Except for the first two cycles, the strain amplitude and the residual strain increment in each cycle are relatively small. The amplitude of ε_{11} is of the order of 10^{-4} and ε_{11} accumulates an amount of the order of 10^{-5} after each cycle. Although a small strain is accumulated after each cycle, the total accumulated strain becomes large after a large number of cycles. Hu et al. [16] also observed strain accumulation in 2D granular samples under low amplitude cyclic loading in their numerical simulations.

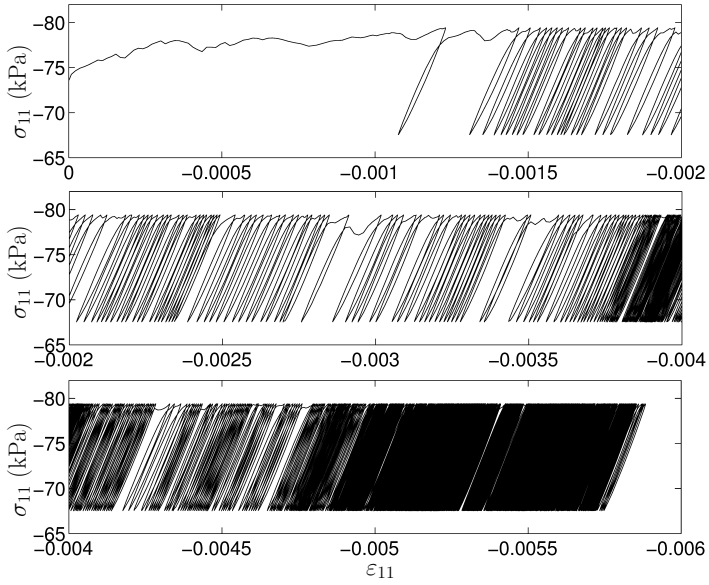

Figure 5: Cyclic axial stress σ_{11} versus axial strain ε_{11} in test B2.

When a granular sample is loaded, the work W_{ext} done by the external loading is converted into (i) kinetic energy E_{k} of the particles, (ii) elastic energy E_{e} stored at the contacts and (iii) energy E_{f} dissipated by frictional sliding between particles and by other dissipative mechanisms such as viscosity and plasticity [18]. The current study assumes that the energy dissipation is only caused by frictional sliding between particles. This assumption might be justified for quasi-static loadings where frictional sliding might be the dominant mechanism. Figure 6 shows the evolution of these quantities for cycles $\mathcal{N} = 1 - 60$. Almost all the work done by the external forces during the cyclic excitation is dissipated by frictional sliding between particles. The kinetic energy of the particles is negligible. Moreover, the elastic energy is completely released after each cycle, except for the first cycle. These results indicate that the strain accumulation phenomenon observed at the macroscale is accompanied by energy dissipation due to frictional sliding at the microscale.

Figure 7 shows the evolution of W_{ext}, E_{e} and E_{f} during two cycles $\mathcal{N} = 60$ and 600. The increments ΔW_{ext}, ΔE_{e}, ΔE_{f} and $\Delta\varepsilon_{11}$ are computed with respect to the beginning of each cycle. Lines AA', BB', CC' and DD' correspond to the beginning of each cycle, the end of the loading phase, the end of the unloading phase and the end of each cycle, respectively. For each loading cycle, the work done by the external loading is converted into elastic energy and dissipated by frictional sliding during the loading phase. The elastic energy is then released and frictional sliding continues to dissipate slightly energy during the unloading phase. At the end of each cycle, the total external work is entirely dissipated by frictional sliding and the elastic energy is completely released. The energy dissipated by frictional sliding remains small compared to the elastic energy during each loading cycle, turning out that the behavior of the sample during low amplitude cyclic

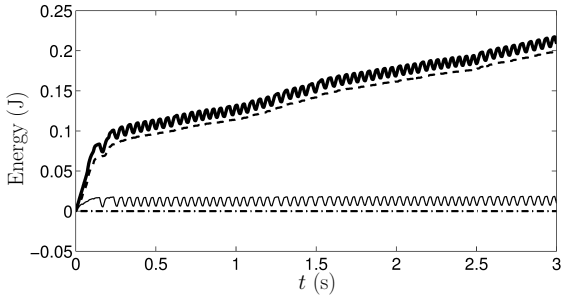

Figure 6: Time history of the external work W_{ext} (bold solid line), kinetic energy E_{k} (dashed-dotted line), elastic energy E_{e} (thin solid line) and energy E_{f} dissipated by friction (dashed line) for cycles $\mathcal{N} = 1 - 60$.

excitation is highly elastic. This would not be the case for large amplitude cyclic excitation, for which frictional sliding would dissipate a large amount of the external work. The behavior of the sample during cycle $\mathcal{N} = 600$ is almost elastic with a negligible dissipated energy compared to that observed for cycle $\mathcal{N} = 60$. This is consistent with the fact that the accumulated strain for cycle $\mathcal{N} = 600$ is much smaller than for cycle $\mathcal{N} = 60$.

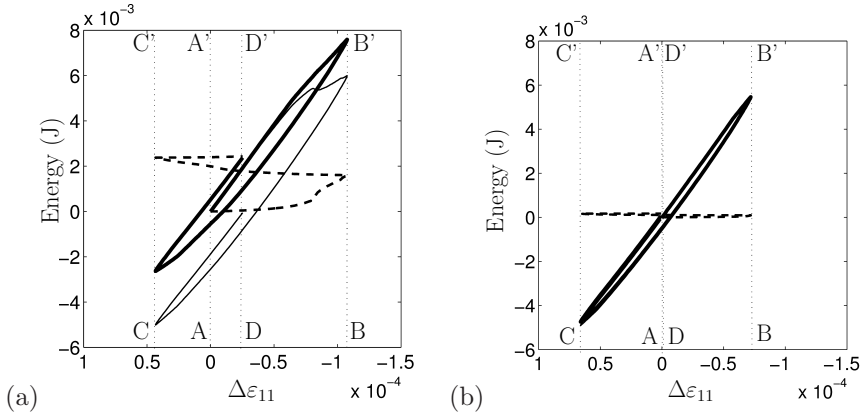

Figure 7: Increments of the external work ΔW_{ext} (bold solid line), elastic energy ΔE_{e} (thin solid line) and energy dissipated by friction ΔE_{f} (dashed line) versus the axial strain increment $\Delta\varepsilon_{11}$ for cycles (a) $\mathcal{N} = 60$ and (b) $\mathcal{N} = 600$.

When a granular sample deforms, frictional sliding occurs at the so-called sliding contacts. Figure 8 shows the evolution of the fraction Φ_{sc} of sliding contacts for cycles $\mathcal{N} = 170 - 181$. Under low amplitude cyclic excitation, the number of sliding contacts in the sample is small ($\Phi_{\text{sc}} < 0.04$); however, these contacts dissipate the main part of energy. Moreover, Φ_{sc} changes periodically. For each cycle, Φ_{sc} increases during the loading phase. Unloading the sample does not lead to disappearance of the sliding contacts; consequently, energy is still dissipated by frictional sliding during this phase. In addition, Φ_{sc} does not decrease monotonically during the unloading phase: it rapidly drops during the first half of the unloading phase, then increases again during the second half. This non-monotonic trend of Φ_{sc} during the unloading phase can be explained by the fact that the sample behaves almost elastically at the transition from the loading to the unloading phase; as a result, Φ_{sc} drops rapidly. As the unloading continues, sliding between particles occurs and Φ_{sc} increases again to dissipate energy. As shown in figure 7, the energy dissipated by frictional sliding increases during the second half of the unloading phase. Figure 8 also shows that the transition from the unloading to the reloading causes Φ_{sc} to drop again (the sample behaves almost elastically at the beginning of the reloading phase). Afterwards, Φ_{sc} increases again to dissipate energy. The periodic variation of the

fraction of sliding contacts during cyclic loading was also observed in [14, 15, 25].

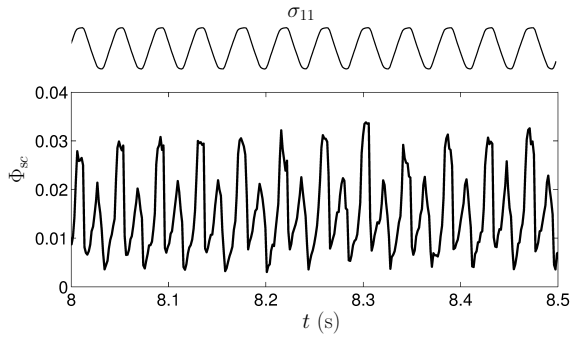

Figure 8: Time history of the fraction Φ_{sc} of sliding contacts for cycles $\mathcal{N} = 170 - 181$.

4.2. Influence of the sample density

The influence of the sample density on the intensity and the direction of strain accumulation as well as the evolution of the internal structure is analyzed by considering test A3 performed on sample A and test B2 performed on sample B. The frequencies of these tests are about 24 Hz. The other parameters are identical (table 3).

The accumulated volumetric and deviatoric strains $\varepsilon_{\mathrm{v}}^{\mathrm{acc}}$ and $\varepsilon_{\mathrm{d}}^{\mathrm{acc}}$ are calculated from the total accumulated strain tensor $\boldsymbol{\varepsilon}^{\mathrm{acc}}$ after each cycle. Figure 9 shows $\varepsilon_{\mathrm{v}}^{\mathrm{acc}}$ and $\varepsilon_{\mathrm{d}}^{\mathrm{acc}}$ for samples A and B versus cycle number $\mathcal{N}$. The sample density influences greatly strain accumulation. Strain accumulates much more strongly in sample A than in sample B. Both samples accumulate more deviatoric than volumetric strain. In particular, sample A accumulates much more volumetric strain than sample B. This means that loose granular soils are more likely to be compacted during low amplitude cyclic loading than dense soils.

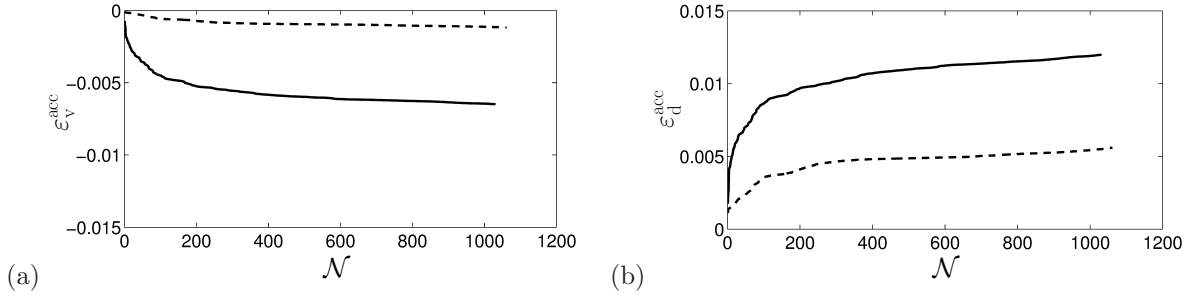

Figure 9: Accumulated (a) volumetric strain $\varepsilon_{\mathrm{v}}^{\mathrm{acc}}$ and (b) deviatoric strain $\varepsilon_{\mathrm{d}}^{\mathrm{acc}}$ versus cycle number $\mathcal{N}$ for samples A (solid line) and B (dashed line).

When plasticity theory is used to predict strain accumulation in granular materials, it is important to know the direction of plastic flow or the direction of strain accumulation [8, 26]. The strain ratio $\varepsilon_{\mathrm{v}}^{\mathrm{acc}}/\varepsilon_{\mathrm{d}}^{\mathrm{acc}}$ is used as a measure of the direction of strain accumulation in a granular sample: it quantifies the change in volume of the sample compared to the change in shear strain and, by definition, takes values between $-3/2$ (the strongest contractive behavior) and $+3/2$ (the strongest dilative behavior). As indicated in figure 10, the direction of strain accumulation in both samples changes first and then stabilizes after about 200 cycles. Moreover, it depends substantially on the sample density: sample A presents a much stronger volumetric behavior during cyclic loading than sample B.

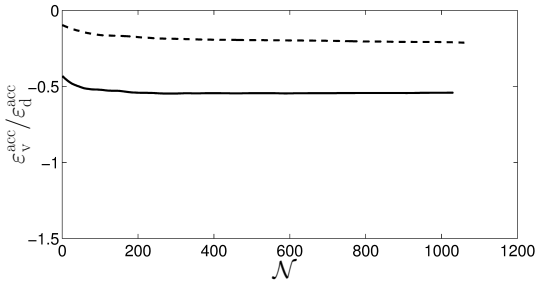

Figure 10: Strain ratio $\varepsilon_{\rm v}^{\rm acc}/\varepsilon_{\rm d}^{\rm acc}$ versus cycle number $\mathcal{N}$ for samples A (solid line) and B (dashed line).

As observed experimentally by many authors [7, 26, 27], the volumetric behavior of a granular sample during cyclic excitation depends on its volumetric behavior at the average stress state. If the sample tends to contract at the average stress state then it contracts during low amplitude cyclic excitation. The opposite is observed if the sample tends to dilate at the average stress state. In particular, if the cyclic excitation is applied at the characteristic state, the strain accumulates in the sample with no volume change. These experimental observations can be confirmed by numerical simulation. Indeed, at point A2 in figure 2, sample A contracts strongly; as a result it contracts strongly during test A3. On the other hand, at point B2 which is near to line $\rm L_B$, sample B contracts weakly during test B2.

To study the evolution of the internal structure of samples A and B during cyclic loading, the effective coordination number $\overline{N}_{\rm eff}$ and the anisotropy measure $H_{\rm d}$ are monitored. Figure 11 shows the evolution of $\overline{N}_{\rm eff}$ and $H_{\rm d}$ for samples A and B. The effective coordination number $\overline{N}_{\rm eff}$ of both samples increases slightly with the number of cycles, particularly for sample A. The increase in $\overline{N}_{\rm eff}$ results from the densification of these samples during cyclic excitation (figure 9). The increase in $\overline{N}_{\rm eff}$ does not mean that the fraction of floating particles decreases during low amplitude cyclic loading. It indeed remains almost constant as shown in figure 12, revealing that low amplitude cyclic loadings do not promote more particles to take part in force chains.

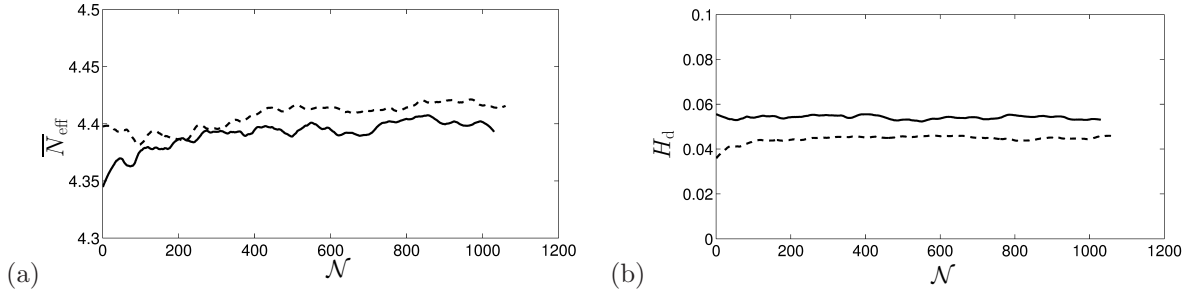

Figure 11: Evolution of (a) the effective coordination number $\overline{N}_{\rm eff}$ and (b) the anisotropy measure $H_{\rm d}$ for samples A (solid line) and B (dashed line).

Figure 11 indicates that the anisotropy of both samples remains almost constant during the applied cyclic excitations. Compared to the anisotropy induced by the consolidation phase, the anisotropy induced by low amplitude cyclic loading is not significant. This result reveals a difference between the effect of cyclic loading with low and high amplitude. For the latter, the internal structure of granular materials evolves substantially [28–30]. Hu et al. [17] studied the evolution of the coordination number and the anisotropy of 2D loose granular materials during low amplitude cyclic loading, revealing similar results as obtained here for 3D materials.

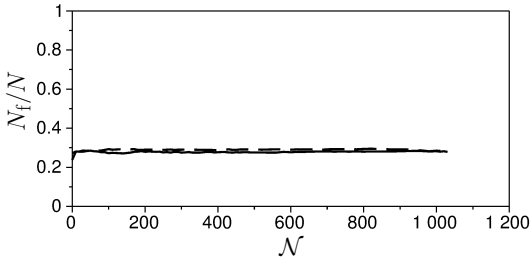

Figure 12: Fraction N_f/N of floating particles versus the number of cycles $\mathcal{N}$ for sample A (solid line) and sample B (dashed line).

4.3. Effect of the cyclic stress amplitude σ_{11}^{cyc}

Tests A2, A3 and A6 are performed on sample A at point A2 with different cyclic stress amplitudes $\sigma_{11}^{cyc} = 3$, 6 and 12 kPa. Figure 13 shows that σ_{11}^{cyc} influences greatly the strain accumulation in sample A. Both accumulated volumetric and deviatoric strains ε_v^{acc} and ε_d^{acc} increase as σ_{11}^{cyc} increases. In addition, at a higher value of σ_{11}^{cyc} strain accumulates more rapidly, particularly for about the first 100 cycles. Hu et al. [17] also observed that the accumulation of the axial strain in 2D materials during low amplitude cyclic loading increases with the cyclic stress amplitude. The increase in ε_v^{acc} and ε_d^{acc} with σ_{11}^{cyc} can be explained by the fact that a higher excitation amplitude causes more sliding motion between particles to dissipate energy. Indeed, figure 14 shows clearly that the energy dissipated by frictional sliding is much higher for $\sigma_{11}^{cyc} = 12$ kPa than for $\sigma_{11}^{cyc} = 6$ kPa.

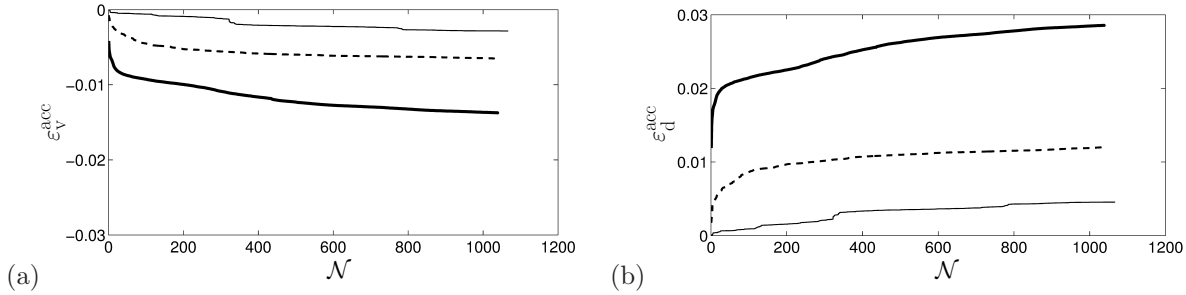

Figure 13: Accumulated (a) volumetric strain ε_v^{acc} and (b) deviatoric strain ε_d^{acc} of sample A versus cycle number $\mathcal{N}$ for a cyclic stress amplitude $\sigma_{11}^{cyc} = 3$ kPa (thin solid line), 6 kPa (dashed line) and 12 kPa (bold solid line).

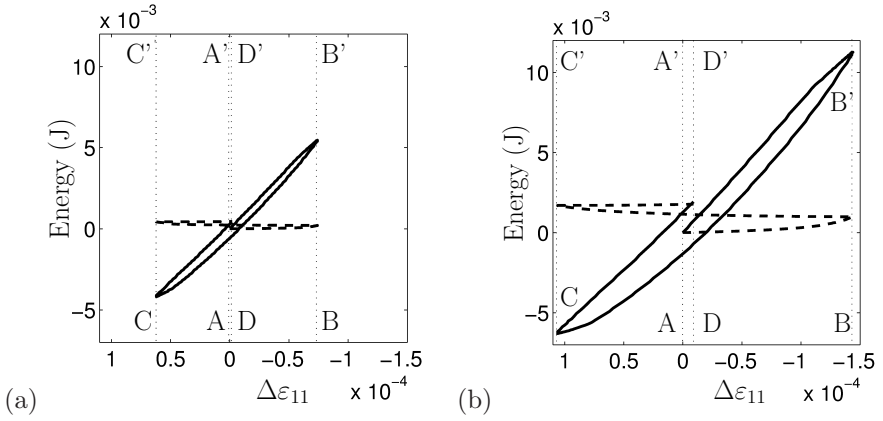

Figure 14: Evolution of the incremental external work ΔW_{ext} (solid line) and the incremental dissipated energy ΔE_{f} (dashed line) during cycle $\mathcal{N} = 600$ for a cyclic stress amplitude (a) $\sigma_{11}^{\text{cyc}} = 6$ kPa and (b) $\sigma_{11}^{\text{cyc}} = 12$ kPa.

The cyclic stress amplitude σ_{11}^{cyc} has little effect on the direction of strain accumulation in sample A, except for the few first cycles, as shown in figure 15. The strain ratio $\varepsilon_{\text{v}}^{\text{acc}}/\varepsilon_{\text{d}}^{\text{acc}}$ after 1000 cycles is about -0.6 for $\sigma_{11}^{\text{cyc}} = 3$ kPa, compared to a value of -0.4 for $\sigma_{11}^{\text{cyc}} = 12$ kPa. This numerical result is in good agreement with the experimental result showing that the direction of strain accumulation in sand under low amplitude cyclic loading is independent of the cyclic excitation amplitude [7, 8, 26].

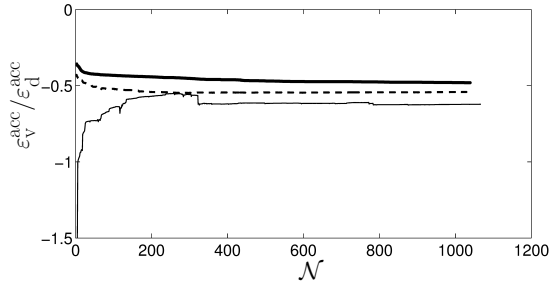

Figure 15: Accumulated strain ratio $\varepsilon_{\text{v}}^{\text{acc}}/\varepsilon_{\text{d}}^{\text{acc}}$ of sample A versus cycle number $\mathcal{N}$ for a cyclic stress amplitude $\sigma_{11}^{\text{cyc}} = 3$ kPa (thin solid line), 6 kPa (dashed line) and 12 kPa (bold solid line).

At the microscopic scale, the cyclic stress amplitude σ_{11}^{cyc} influences significantly the evolution of the effective coordination number $\overline{N}_{\text{eff}}$ of sample A, as indicated in figure 16. A marked increase of $\overline{N}_{\text{eff}}$ is observed for $\sigma_{11}^{\text{cyc}} = 12$ kPa, while $\overline{N}_{\text{eff}}$ remains almost constant for $\sigma_{11}^{\text{cyc}} = 3$ kPa. The dependence of $\overline{N}_{\text{eff}}$ on σ_{11}^{cyc} results from the fact that the sample densifies more strongly at a higher value of σ_{11}^{cyc} (figure 13).

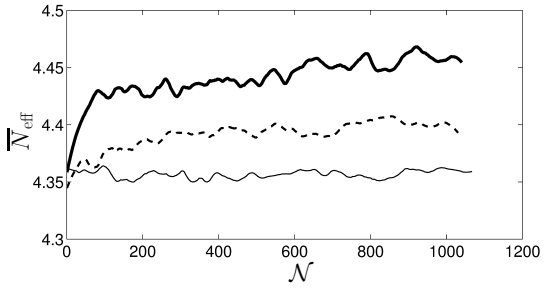

Figure 16: Effective coordination number $\overline{N}_{\rm eff}$ of sample A versus cycle number $\mathcal{N}$ for a cyclic stress amplitude $\sigma_{11}^{\rm cyc} = 3$ kPa (thin solid line), 6 kPa (dashed line) and 12 kPa (bold solid line).

4.4. Influence of the cyclic excitation frequency f

Tests A3, A4 and A5 are performed on sample A at different excitation frequencies $f = 24$, 67 and 93 Hz and tests B2, B3 and B4 are performed on sample B at $f = 25$, 68 and 100 Hz. The magnitude $\varepsilon^{\rm acc}$ of the accumulated strain is plotted versus the cycle number $\mathcal{N}$ for samples A and B in figure 17. The cyclic excitation frequency f has little effect on strain accumulation in these samples. For sample A, $\varepsilon^{\rm acc}$ is about 0.015 at 24 Hz after 1000 cycles, compared to a value of 0.016 at 93 Hz. This result might be explained by the fact that, for the considered values of the excitation frequency, samples A and B are still in the quasi-static regime. Monitoring the unbalanced force ratio $I_{\rm uf}$ introduced by Ng [31] shows that $I_{\rm uf} < 10^{-2}$ throughout the performed tests, which is small enough for a quasi-static loading. Moreover, the kinetic energy $E_{\rm k}$ is negligible compared to the external work $W_{\rm ext}$ during the performed tests ($E_{\rm k}/W_{\rm ext} < 10^{-4}$).

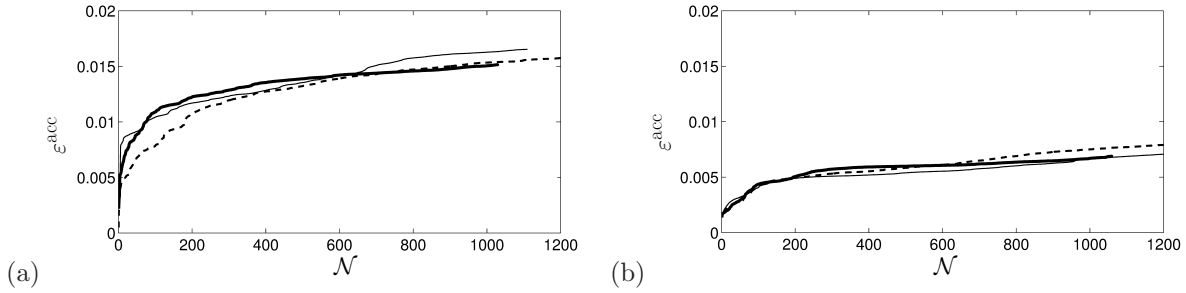

Figure 17: Accumulated strain $\varepsilon^{\rm acc}$ versus cycle number $\mathcal{N}$ (a) for sample A at a cyclic excitation frequency 24 Hz (bold solid line), 67 Hz (dashed line) and 93 Hz (thin solid line) and (b) for sample B at 25 Hz (bold solid line), 68 Hz (dashed line) and 100 Hz (thin solid line).

In the literature, reports on the effect of the cyclic excitation frequency on strain accumulation in granular materials are contradictory. Karg [6] found that the frequency within the range 0.1 Hz $\leq f \leq$ 10 Hz does not have a significant influence on strain accumulation in sand samples. A similar result was found by Shenton [32] on ballast samples with frequencies 0.1 Hz $\leq f \leq$ 30 Hz. On the other hand, a clear dependence of strain accumulation in ballast samples on the frequency within the range 10 Hz $\leq f \leq$ 40 Hz was observed by Indraratna et al. [11]. This experimental observation was also confirmed by numerical simulations performed with the DEM. The question is why such a dependence is not found in our simulations. This might be explained by two reasons. The first reason is that the particles considered in our simulations are much smaller than those considered in [11] in which the particle diameter varies from 19 mm to 45 mm. In view of the inertial effect, the latter are more sensitive to the loading rate than the former. The second reason is that the cyclic excitation amplitude considered in [11] is much larger than in our simulations.

The time step used to simulate samples A and B is about 1.5×10^{-6} s. As a result, about 27000 steps

are needed for each loading cycle at 25 Hz, which is computationally expensive. To save computation time, cyclic loading tests at higher frequencies 60 Hz $< f <$ 70 Hz are considered in the sequel of this paper.

4.5. Effect of the average stress ratio $\overline{\eta}$

Tests A1, A4 and A8 on sample A at points A1, A2 and A3 and tests B1, B3 and B5 on sample B at points B1, B2 and B3 are considered to analyze the effect of the average stress ratio $\overline{\eta}$ on strain accumulation. Note that $\overline{\eta} = 0.2$ at points A1 and B1, $\overline{\eta} = 0.4$ at points A2 and B2 and $\overline{\eta} = 0.6$ at points A3 and B3 (figure 2). These tests are performed at a high frequency of approximately 65 Hz. The number of cycles is about 8000 for the tests performed on sample A and 2000 for the tests performed on sample B.

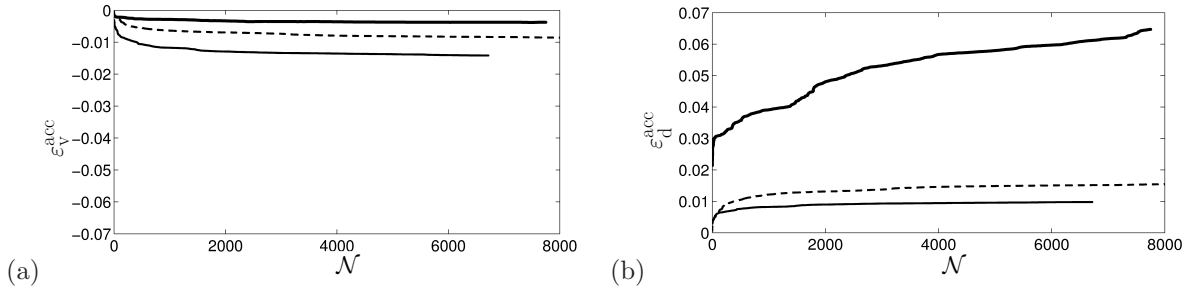

Figure 18: Accumulated (a) volumetric strain ε_v^{acc} and (b) deviatoric strain ε_d^{acc} versus cycle number $\mathcal{N}$ for sample A at an average stress ratio $\overline{\eta} = 0.2$ (thin solid line), 0.4 (dashed line) and 0.6 (bold solid line).

The accumulated strain in sample A depends strongly on the average stress ratio $\overline{\eta}$, particularly for the accumulated deviatoric strain ε_d^{acc}, as indicated in figure 18. Strain accumulates much more strongly in sample A for $\overline{\eta} = 0.6$ than for $\overline{\eta} = 0.2$ and 0.4, in particular for the first 10 cycles. After 6000 cycles, ε_d^{acc} reaches a large value of 0.06 for $\overline{\eta} = 0.6$, compared to a value of 0.015 for $\overline{\eta} = 0.4$ and 0.01 for $\overline{\eta} = 0.2$. In addition, for $\overline{\eta} = 0.6$ strain still accumulates substantially in sample A after 7000 cycles, while for $\overline{\eta} = 0.2$ and 0.4, strain accumulation almost ceases after 1000 cycles.

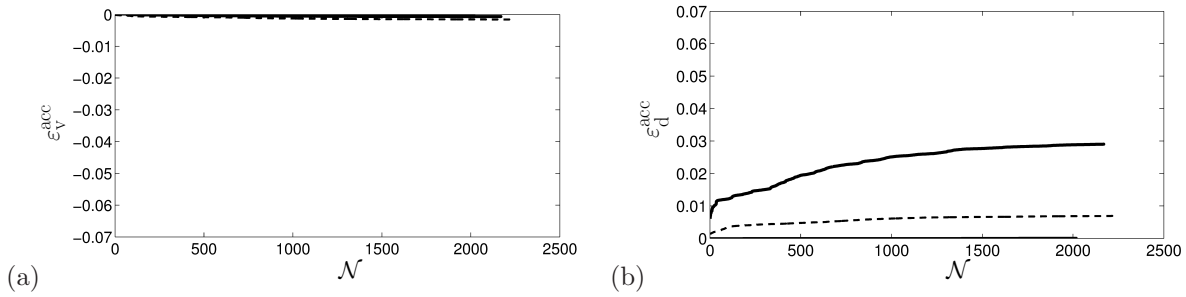

Figure 19: Accumulated (a) volumetric strain ε_v^{acc} and (b) deviatoric strain ε_d^{acc} versus cycle number $\mathcal{N}$ for sample B at an average stress ratio $\overline{\eta} = 0.2$ (thin solid line), 0.4 (dashed line) and 0.6 (bold solid line).

A similar effect of the average stress ratio $\overline{\eta}$ on strain accumulation is observed on sample B (figure 19). The accumulated volumetric strain ε_v^{acc} is negligible compared to the deviatoric strain ε_d^{acc}. The accumulated strain is almost zero during the cyclic excitation applied at $\overline{\eta} = 0.2$ as the behavior of sample B is highly elastic at this average stress state (figure 2). These results mean that strain accumulation during low amplitude cyclic loading in granular materials depends strongly on stress history, which has also been found in [17].

Figure 18 also shows that, for a higher value of the average stress ratio $\overline{\eta}$, sample A accumulates more deviatoric strain ε_d^{acc} but less volumetric strain ε_v^{acc}. For $\overline{\eta} = 0.6$, ε_v^{acc} is very small compared to ε_d^{acc}, while

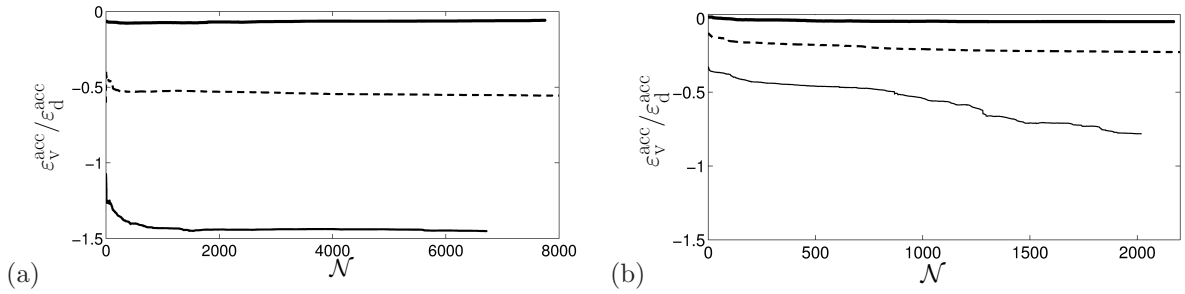

Figure 20: Accumulated strain ratio $\varepsilon_{\rm v}^{\rm acc}/\varepsilon_{\rm d}^{\rm acc}$ versus cycle number $\mathcal{N}$ for samples (a) A and (b) B at an average stress ratio $\overline{\eta}$ = 0.2 (thin solid line), 0.4 (dashed line) and 0.6 (bold solid line).

these quantities are comparable for $\overline{\eta} = 0.2$. This result means that $\overline{\eta}$ affects greatly the direction of strain accumulation in sample A as shown in figure 20 where the accumulated strain ratio $\varepsilon_{\rm v}^{\rm acc}/\varepsilon_{\rm d}^{\rm acc}$ is plotted versus the cycle number $\mathcal{N}$. For $\overline{\eta} = 0.2$, $\varepsilon_{\rm v}^{\rm acc}/\varepsilon_{\rm d}^{\rm acc}$ is near to its minimum value of -3/2 (maximum contractive behavior). On the other hand, $\varepsilon_{\rm v}^{\rm acc}/\varepsilon_{\rm d}^{\rm acc}$ is near to 0 for $\overline{\eta} = 0.6$, meaning that sample A accumulates only the deviatoric strain at this average stress state. A similar result is observed for sample B, although the influence of $\overline{\eta}$ on the direction of strain accumulation is less marked than in sample A.

These results demonstrate the close relation between the direction of strain accumulation in a granular sample at a given average stress state and its volumetric behavior at this stress state, as mentioned earlier in subsection 4.2. The strong contractive behavior of sample A at point A1 leads to a strong accumulation of the volumetric strain and a weak accumulation of the deviatoric stress, while its weak contractive behavior at point A3 leads to a weak accumulation of the volumetric strain and a strong accumulation of the deviatoric strain. These results are in accordance with experimental results obtained by Luong [27], Chang and Whitman [26] and Wichtmann et al. [7, 8] who showed a strong dependence of strain accumulation in sand samples on the average stress ratio.

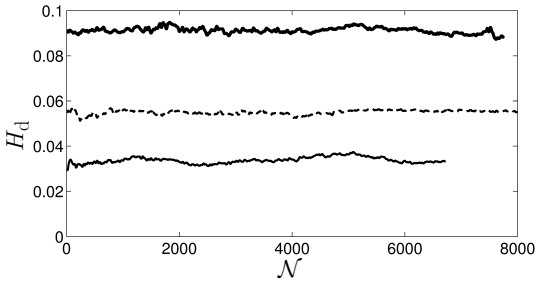

Figure 21: Anisotropy measure $H_{\rm d}$ versus cycle number $\mathcal{N}$ for sample A at an average stress ratio $\overline{\eta} = 0.2$ (thin solid line), 0.4 (dashed line) and 0.6 (bold solid line).

The effect of the average stress ratio $\overline{\eta}$ on the evolution of the anisotropy of sample A is shown in figure 21. The average stress ratio $\overline{\eta}$ affects greatly the anisotropy induced by the consolidation phase, but not the anisotropy induced by low amplitude cyclic excitation. The anisotropy of the sample remains almost constant during the applied cylic excitations whatever the value of $\overline{\eta}$ is. This result confirms what has been observed previously in subsection 4.2.

4.6. Influence of the confinement stress $\sigma_{\rm o}$

Tests A4 and A7 are performed on sample A at point A2 with different confinement stresses $\sigma_{\rm o} = 50$ kPa and 100 kPa. The cyclic stress amplitude $\sigma_{11}^{\rm cyc}$ is chosen such that the parameter $\zeta^{\rm cyc} = \sigma_{11}^{\rm cyc}/\mid \overline{p} \mid = 0.1$ for

both tests; hence $\sigma_{11}^{\mathrm{cyc}} = 6$ kPa for test A4 and $\sigma_{11}^{\mathrm{cyc}} = 12$ kPa for test A7. Figure 22 shows the accumulated strain in sample A at both values of σ_{o}. The strain accumulates less at $\sigma_{\mathrm{o}} = 100$ kPa than at $\sigma_{\mathrm{o}} = 50$ kPa, although the cyclic stress amplitude $\sigma_{11}^{\mathrm{cyc}}$ is higher for the former than for the latter. However, as shown in figure 23, the confinement stress has little influence on the direction of strain accumulation except for some first cycles. These results indicate that an increase in the confinement stress tends to reduce strain accumulation in granular samples during low amplitude cyclic excitation without changing remarkably the direction of strain accumulation. A similar result was also observed in laboratory experiments by Wichtmann et al. [7, 8].

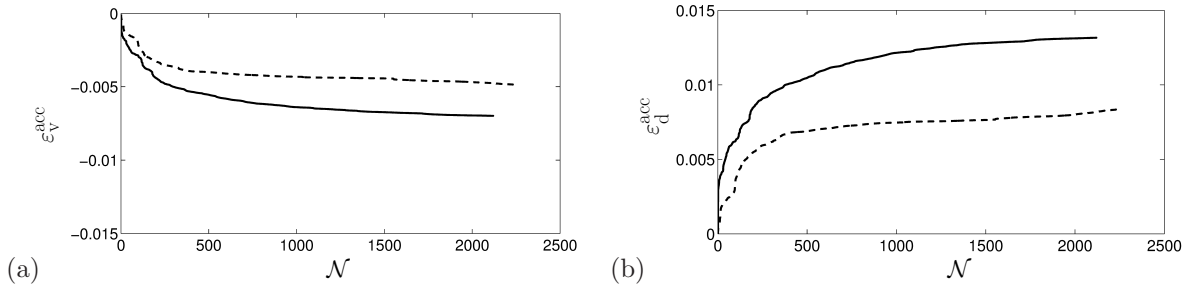

Figure 22: Accumulated (a) volumetric strain $\varepsilon_{\mathrm{v}}^{\mathrm{acc}}$ and (b) deviatoric strain $\varepsilon_{\mathrm{d}}^{\mathrm{acc}}$ versus cycle number $\mathcal{N}$ for sample A at a confinement stress $\sigma_{\mathrm{o}} = 50$ kPa (solid line) and 100 kPa (dashed line).

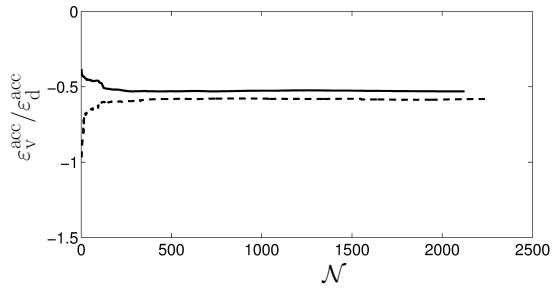

Figure 23: Accumulated strain ratio $\varepsilon_{\mathrm{v}}^{\mathrm{acc}}/\varepsilon_{\mathrm{d}}^{\mathrm{acc}}$ versus cycle number $\mathcal{N}$ for sample A at a confinement stress $\sigma_{\mathrm{o}} = 50$ kPa (solid line) and 100 kPa (dashed line).

5. Conclusions

A series of simulations with the DEM was carried out to study strain accumulation in granular materials subjected to low amplitude cyclic loading. While cyclic triaxial tests at high frequency are difficult to perform in the laboratory, they can easily be simulated with the DEM. A loose and a medium dense sample composed of 10342 spheres were considered in these simulations. The influence of different factors such as the packing density, the cyclic stress amplitude, the excitation frequency and the average stress state on strain accumulation in these samples was analyzed. In addition, the DEM allowed the study of the energetic behavior and the evolution of the internal structure of these samples during the performed cyclic loading tests. Although the granular samples considered in this study are somewhat idealized, the following conclusions regarding strain accumulation in granular materials during low amplitude cyclic loading at high frequency can be formulated:

- Strain accumulation in granular samples under low amplitude cyclic loading is clearly observed in the performed simulations.

- Strain accumulation observed at the macroscale is accompanied by a dissipative process caused by frictional sliding occurring at a few contacts. The fraction of sliding contacts varies periodically during cyclic excitation.
- During each low amplitude loading cycle, the behavior of these samples is highly elastic and a small amount of energy is dissipated by frictional sliding. However, after a large number of loading cycles, the amount of cumulative dissipated energy becomes substantial compared to the elastic energy which is completely released after each cycle.
- The internal structure of these samples evolves slightly during the performed cyclic loading tests. An increase in the coordination number observed for the loose sample is due to its densification during cyclic excitation. However, the anisotropy of these samples induced by low amplitude cyclic excitation is negligible compared to the anisotropy induced by the consolidation phase.
- Strain accumulation in granular samples depends greatly on the packing density, the excitation amplitude and the average stress state. This dependence was also observed in laboratory experiments. The excitation frequency (up to 100 Hz), however, does not substantially affect strain accumulation. It appears that the considered samples are still in quasi-equilibrium during the performed cyclic loading tests within this range of frequencies.

These results indicate that the DEM is able to reproduce, at least in a qualitative sense, the strain accumulation phenomenon observed in laboratory experiments. To advance the use of the DEM to study this topic, more realistic particle shapes and more realistic boundary conditions such as the stress-controlled membrane should be accounted for in simulations. Crushable particles should be considered in the case of low amplitude cyclic tests at high confinement stress to investigate whether particle breakage plays an important role in strain accumulation. Moreover, the effect of some properties at the microscopic scale such as the friction coefficient, the particle size distribution, the particle shape and the initial fabric of granular materials on strain accumulation in these media is not yet well understood and needs to be further investigated.

Acknowledgements

The results presented in this paper have been obtained within the frame of the FWO project G.0397.09 "The constitutive behaviour of granular soils under repeated dynamic loading". The second author is a post-doctoral fellow of the Research Foundation Flanders (FWO). The support of FWO is gratefully acknowledged.

[1] G. Lombaert and G. Degrande. The experimental validation of a numerical model for the prediction of the vibrations in the free field produced by road traffic. *Journal of Sound and Vibration*, 262:309–331, 2003.

[2] G. Lombaert, G. Degrande, J. Kogut, and S. François. The experimental validation of a numerical model for the prediction of railway induced vibrations. *Journal of Sound and Vibration*, 297:512–535, 2006.

[3] S. François, C. Karg, W. Haegeman, and G. Degrande. A numerical model for foundation settlements due to deformation accumulation in granular soils under repeated small amplitude dynamic loading. *International Journal for Numerical and Analytical Methods in Geomechanics*, 34:273–296, 2010.

[4] A. Niemunis, T. Wichtmann, and T. Triantafyllidis. A high-cycle accumulation model for sand. *Computers and Geotechnics*, 32:245–263, 2005.

[5] A.S.J. Suiker and R. de Borst. A numerical model for the cyclic deterioration of railway tracks. *International Journal for Numerical Methods in Engineering*, 57:441–470, 2003.

[6] C. Karg. *Modelling of strain accumulation due to low level vibrations in granular soils.* PhD thesis, Ghent University, Ghent, Belgium, 2007.

[7] T. Wichtmann, A. Niemunis, and T. Triantafyllidis. Strain accumulation in sand due to cyclic loading: drained triaxial tests. *Soil Dynamics and Earthquake Engineering*, 25:967–979, 2005.

[8] T. Wichtmann. *Explicit accumulation model for non-cohesive soils under cyclic loading.* PhD thesis, Des Institutes Für Grundbau Und Bodenmechanik Der Ruhr-Universität-Bochum, Bochum, Germany, 2005.

[9] E. Rascol. *Cyclic properties of sand: Dynamic behaviour for seismic applications.* PhD thesis, Ecole Polytechnique Fédérale de Lausanne, Lausanne, Switzerland, 2009.

[10] A.S.J. Suiker. *The mechanical behaviour of ballasted railway tracks.* PhD thesis, Delft University of Technology, Delft, The Netherlands, 2002.

[11] B. Indraratna, P.K. Thakur, and J.S. Vinod. Experimental and numerical study of railway ballast behavior under cyclic loading. *International Journal of Geomechanics*, 10:136–144, 2010.
[12] P.A. Cundall and O.D.L. Strack. A discrete numerical model for granular assemblies. *Géotechnique*, 29(1):47–65, 1979.
[13] C. O'Sullivan. *Particulate Discrete Element Modelling: A Geomechanics Perspective*. Applied Geotechnics Volume 4. Spon Press, 2011.
[14] F. Alonso-Marroquín and H.J. Herrmann. Ratcheting of granular materials. *Physical Review Letters*, 92(5):054301(4), 2004.
[15] F. Alonso-Marroquín, H.B. Mühlhaus, and H.J. Herrmann. Micromechanical investigation of granular ratcheting using a discrete model of polygonal particles. *Particuology*, 6(6):390–403, 2008.
[16] M. Hu, C. O'Sullivan, R.R. Jardine, and M. Jiang. Study on the deformation of loose sand under cyclic loading by DEM simulation. In R. Meier, A. Abbo, and L. Wang, editors, *Soil Behavior and Geo-Micromechanics*, pages 212–219. American Society of Civil Engineers, 2010.
[17] M. Hu, C. O'Sullivan, R.R. Jardine, and M. Jiang. Stress-induced anisotropy in sand under cyclic loading. *Granular Matter*, 12:469–476, 2010.
[18] Itasca Consulting Group Inc. *PFC3D: Theory and Background*, 2008.
[19] S. Donohue, C. O'Sullivan, and M. Long. Particle breakage during cyclic triaxial loading of a carbonate sand. *Géotechnique*, 59(5):477–482, 2009.
[20] T.-T. Ng. Triaxial test simulations with discrete element method and hydrostatic boundaries. *Journal of Engineering Mechanics*, 130(10):11881194, 2004.
[21] G. Cheung and C. O'Sullivan. Effective simulation of flexible lateral boundaries in two- and three-dimensional dem simulations. *Particuology*, 6:483500, 2008.
[22] M.R. Kuhn. Structured deformation in granular materials. *Mechanics of Materials*, 31:407–429, 1999.
[23] M. Satake. Fabric tensor in granular materials. In P. Vermeer and H. Luger, editors, *IUTAM Symposium on Deformation and Failure of Granular Materials*, pages 63–68. A.A. Balkema, 1982.
[24] E. Vincens and C. Nouguier-Lehon. The characteristic state. *European Journal of Environmental and Civil Engineering*, 16(7):777–794, 2012.
[25] S. Luding, C.T. David, R. García-Rojo, and H.J. Herrmann. Frictional powders: Ratcheting under periodic strain in 3D. In *Partec 2007*, Nuremberg, Germany, 27–29 March 2007.
[26] C.S. Chang and R.V. Whitman. Drained permanent deformation of sand due to cyclic loading. *Journal of Geotechnical Engineering*, 114:1164–1180, 1988.
[27] M.P. Luong. Mechanical aspects and thermal effects of cohesionless soils under cyclic and transient loading. In *IUTAM Conference on Deformation and Failure of Granular Materials*, pages 239–246, Delft, 1982.
[28] C. O'Sullivan, L. Cui, and S. O'Neill. Discrete element analysis of the response of granular materials during cyclic loading. *Soils and Foundations, the Japanese Geotechnical Society*, 48(4):511–530, 2008.
[29] Y. Yunus, E. Vincens, and B. Cambou. Numerical local analysis of relevant internal variables for constitutive modelling of granular materials. *International Journal for Numerical and Analytical Methods in Geomechanics*, 34:1101–1123, 2010.
[30] M.M. Sazzad and K. Suzuki. Effect of interparticle friction on the cyclic behavior of granular materials using 2D DEM. *Journal of Geotechnical and Geoenvironmental Engineering*, 137(5):545–549, 2011.
[31] T.-T. Ng. Input parameters of discrete element methods. *ASCE Journal of Engineering Mechanics*, 132(7):723–729, 2006.
[32] M.J. Shenton. Deformation of railway ballast under repeated loading conditions. In *Railroad track mechanics and technology*, pages 405–425. Pergamon Press, 1978.